

Superconductivity at 23 K and Low Anisotropy in Rb-Substituted BaFe₂As₂ Single Crystals

Z. Bukowski^{1,*}, S. Weyeneth², R. Puzniak³, P. Moll¹, S. Katrych¹,

N. D. Zhigadlo¹, J. Karpinski¹, H. Keller², and B. Batlogg¹

¹ Laboratory for Solid State Physics, ETH Zurich, CH-8093 Zurich, Switzerland

² Physik-Institut der Universität Zürich, Winterthurerstrasse 190, CH-8057 Zürich, Switzerland

³ Institute of Physics, Polish Academy of Sciences,

Aleja Lotników 32/46, PL-02-668 Warsaw, Poland

Single crystals of Ba_{1-x}Rb_xFe₂As₂ with $x = 0.05 - 0.1$ have been grown from Sn flux and are bulk superconductors with T_c up to 23 K. The crystal structure was determined by X-ray diffraction analysis, and Sn is found to be incorporated for $\sim 9\%$ Ba, shifted by ~ 1.1 Å away from the Ba site towards the (Fe₂As₂)-layers. The upper critical field deduced from resistance measurements is anisotropic with slopes of 7.1(3) T/K ($H||ab$ -plane) and 4.2(2) T/K ($H||c$ -axis), sufficiently far below T_c . The extracted upper critical field anisotropy $\gamma_H \sim 3$ close to T_c , is in good agreement with the estimate from magnetic torque measurements. This indicates that the electronic properties in the doped BaFe₂As₂ compound are significantly more isotropic than those in the *Ln*FeAsO family. The in-plane critical current density at 5 K exceeds 10^6 A/cm², making Ba_{1-x}Rb_xFe₂As₂ a promising candidate for technical applications.

PACS numbers: 74.70.Dd, 74.25.-q, 74.25.Op, 61.05.cp

I. INTRODUCTION

The report on superconductivity at 5 K in LaFePO with the ZrCuSiAs-type structure by Kamihara *et al.*¹ was almost overlooked for two years until the discovery of superconductivity at $T_c \simeq 26$ K in F-substituted LaFeAsO.² This finding initiated an intensive search for new FeAs-based superconductors and in the few following months superconductivity has been discovered in a number of analogues, primarily by substituting other rare earth ions for La, yielding its current maximum $T_c \simeq 56$ K for SmFeAsO_{1-x}F_x.³ The crystal structure of *Ln*FeAsO (abbreviated as “1111”) consists of (Fe₂As₂)-layers sandwiched by (*Ln*₂O₂)-layers, where *Ln* denotes any lanthanide element. The parent compound *Ln*FeAsO is antiferromagnetic, but may become superconducting upon electron doping by either partially replacing oxygen by fluorine, by generating oxygen deficiency, or by applying pressure.⁴ Superconductivity can be also induced in *Ln*FeAsO through electron doping (partially replacing *Ln* by Th⁵) or hole doping (partially replacing *Ln* by Sr⁶).

More recently, the discovery of superconductivity at 38 K in Ba_{1-x}K_xFe₂As₂ with the ThCr₂Si₂-type structure has been reported.⁷ The *A*Fe₂As₂ (*A* = Ca, Sr, Ba) compounds (called “122”) have a more simple crystal structure in which (Fe₂As₂)-layers, identical to those in *Ln*FeAsO, are separated by single elemental *A* layers. Thus, a new class of superconductors was established by the subsequent reports on superconductivity in isostructural hole-doped Sr_{1-x}K_xFe₂As₂ and Sr_{1-x}Cs_xFe₂As₂,⁸ Ca_{1-x}Na_xFe₂As₂,⁹ Eu_{1-x}K_xFe₂As₂ and Eu_{1-x}Na_xFe₂As₂,^{10,11} and in electron-doped Co-substituted BaFe₂As₂ and SrFe₂As₂,^{12,13} and Ni-substituted BaFe₂As₂.¹⁴ Furthermore, pressure induced superconductivity has been discovered in the parent com-

pounds CaFe₂As₂,^{15,16} SrFe₂As₂,^{17,18} and BaFe₂As₂.¹⁸

Besides KFe₂As₂ and CsFe₂As₂, which are superconductors with T_c 's of 3.8 K and 2.6 K,⁸ respectively, RbFe₂As₂ is known to exist as well.¹⁹ Therefore, it seemed natural to us using Rb as a chemical substituent in order to extend the number of elements which can effectively induce superconductivity in *A*Fe₂As₂ compounds. In this paper, we report on the superconduc-

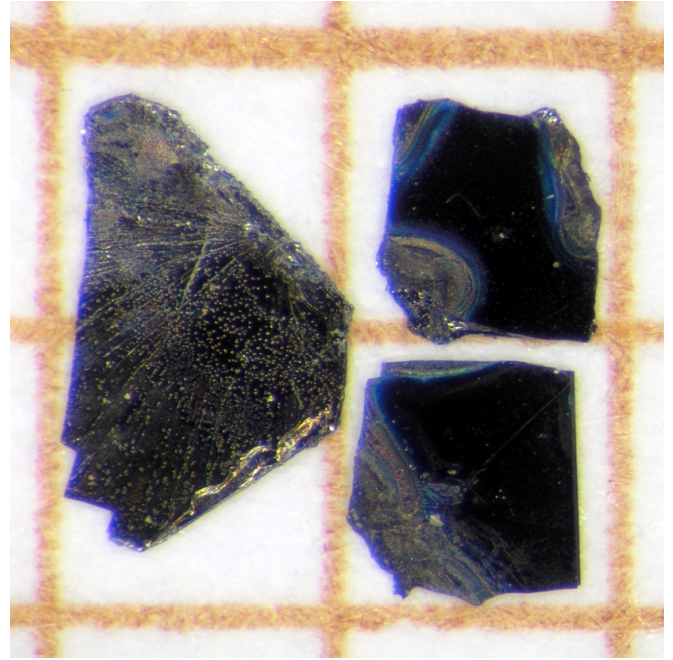


FIG. 1: (Color online) Photograph of three single crystals of Ba_{0.84}Rb_{0.10}Sn_{0.09}Fe₂As_{1.96} on a millimeter grid.

tivity induced in BaFe_2As_2 by partial substitution of Rb for Ba, and present its basic superconducting properties, including estimates of the electronic anisotropy.

II. EXPERIMENTAL DETAILS

Single crystals of Rb substituted BaFe_2As_2 $[(\text{Ba},\text{Rb})_{122}]$ were grown using a Sn flux method similar to that described by Ni *et al.*²⁰ The Fe:Sn ratio (1:24) in a starting composition was kept constant in all runs while the Rb:Ba ratio was varied between 0.7 and 2.0. The appropriate amounts of Ba, Rb, Fe_2As , As, and Sn were placed in alumina crucibles and sealed in silica tubes under 1/3 atmosphere of Ar gas. Next, the ampoules were heated at 850 °C for 3 hours until all components were completely melted, and cooled to 500 °C in 50 hours. At this temperature the ampoule was turned upside down inside a furnace and liquid Sn was decanted from the crystals. The remaining thin film of Sn at the crystal surfaces was subsequently dissolved at room temperature by soaking crystals for a few days in liquid Hg. Finally, the crystals were heated for one hour at 190 °C in vacuum to evaporate the remaining traces of Hg. No signs of superconducting Hg are seen in the magnetic measurements.

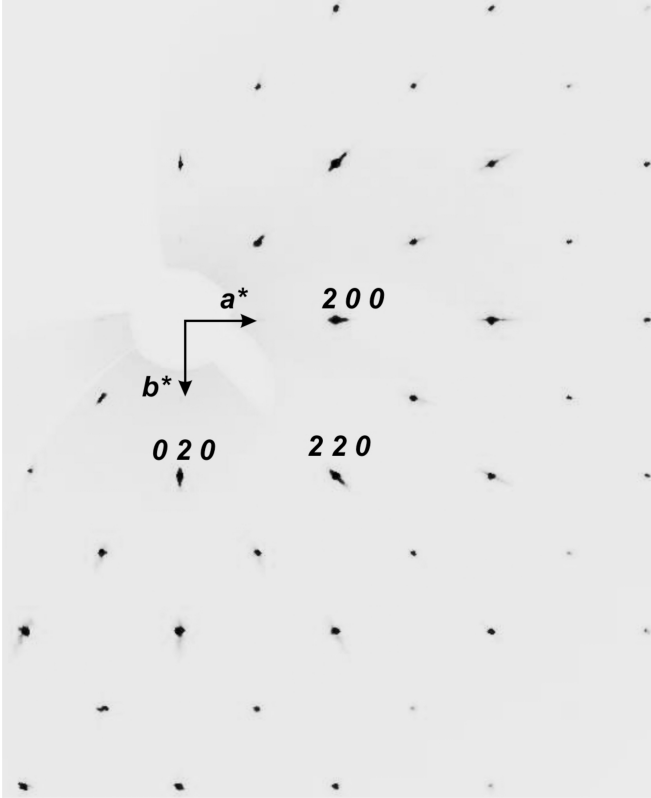


FIG. 2: The $hk0$ reciprocal space section determined by XRD of the single crystal $\text{Ba}_{0.84}\text{Rb}_{0.10}\text{Sn}_{0.09}\text{Fe}_2\text{As}_{1.96}$.

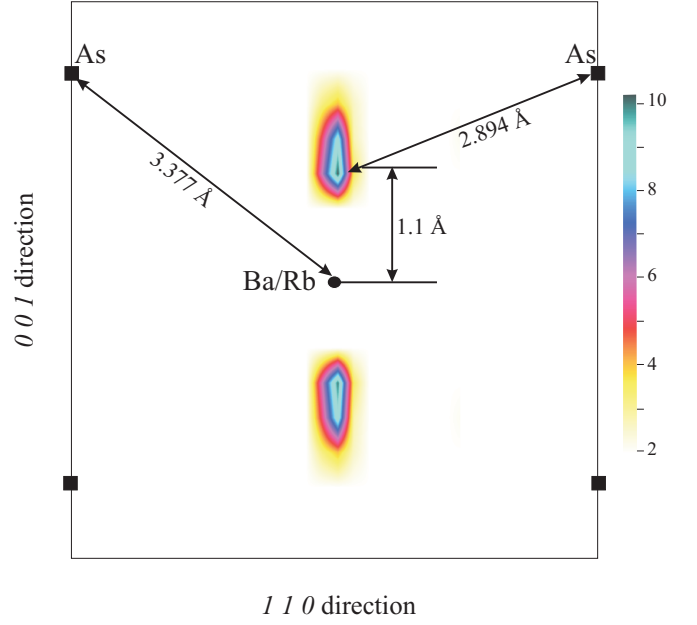


FIG. 3: (Color online) 110 section of the $F_0 - F_c$ difference Fourier map. The enhanced electron density reveals the location of Sn atoms, shifted by 1.1 Å towards the (Fe_2As_2) -layers. The black dot shows the Ba/Rb position and black squares mark the As positions.

The phase purity was checked on crushed crystals by means of powder X-ray diffraction (XRD) measurements carried out on a STOE diffractometer using $\text{Cu-K}\alpha$ radiation and a graphite monochromator.

Single-crystal X-ray diffraction data were collected on a 4-circle diffractometer equipped with a CCD detector (Oxford Diffraction Ltd, $\text{Mo-K}\alpha$, 60 mm sample to detector distance). Data reduction and analytical absorption correction were applied using the CrysAlis RED software package.²¹ The crystal structure was refined on F^2 employing the SHELXL program.²² The starting model for the refinement was taken from Ref.²³ The elemental analysis of the crystals was performed by means of energy dispersive X-ray (EDX) spectrometry.

Magnetic measurements were performed in a Quantum Design Magnetic Property Measurement System (MPMS XL) with the Reciprocating Sample Option (RSO) installed. Transport measurements were performed in a 14 Tesla Quantum Design Physical Property Measurement System (PPMS). Magnetic torque measurements were carried out by using a highly sensitive miniaturized piezoresistive torque sensor within a home made experimental set-up described elsewhere.^{24,25}

III. RESULTS AND DISCUSSION

The single crystals of $\text{Ba}_{1-x}\text{Rb}_x\text{Fe}_2\text{As}_2$ grow in a plate-like shape with typical dimensions (1-3) x (1-2) x (0.05-

0.1) mm³ (see Fig. 1). Depending on the starting composition, the crystals displayed a broad variety of properties from non-superconducting to superconducting with rather sharp transitions to the superconducting state. For further studies we chose single crystals grown from the starting composition Ba_{0.6}Rb_{0.8}Fe₂As₂. The composition of the crystals from this batch determined by EDX analysis (16.79 at.% Ba, 1.94 at.% Rb, 1.74 at.% Sn, 40.19 at.% Fe, and 39.33 at.% As) leads to the chemical formula Ba_{0.84}Rb_{0.10}Sn_{0.09}Fe₂As_{1.96}. Crystals from the selected batch exhibit a T_c around 23 K but compared to the crystals with higher T_c their superconducting transition is relatively sharp, suggesting superior quality.

A. Crystal structure

The crystals studied by XRD are of good quality, and no additional phases (impurities, twins or intergrowing crystals) were detected by examining the reconstructed reciprocal space sections (see Fig. 2). The average mosaic spread of 1.45° was estimated using the XCalibur, CrysAlis Software System by analyzing all frames.²¹

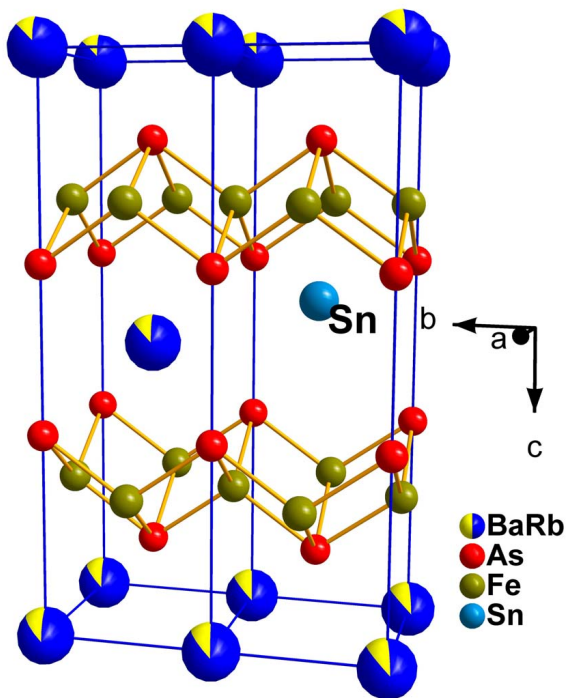


FIG. 4: (Color online) Schematic illustration of two unit cells of Rb and Sn substituted BaFe₂As₂. The possible Sn location is shown, for clarity, on one site only.

We assumed that Rb atoms substitute for Ba atoms and the Rb/Ba occupations have been refined simultaneously. The content of these elements was found to be 1.0 at.% (Rb) and 17.8 at.% (Ba), in acceptable agreement with the EDX analysis (1.9 at.% Rb and 16.8 at.% Ba).

It has been reported that the BaFe₂As₂ crystals grown from a Sn flux have approximately 1 at.% of Sn incorporated into the structure with the Sn atoms most likely located on the As sites.²⁰ However, our structure refinement reveals a somewhat different picture. After several cycles of refinement the Fourier difference map shows two pronounced maxima of the electron density away from the Ba/Rb site. We located the Sn atoms on these sites, shifted towards the (Fe₂As₂)-layers (Fig. 3). This interpretation is supported by the considerable reduction of the R factor from 5.41 % to 3.89 % when Sn atoms are allowed to occupy these “off-center” sites. The resulting distances to the As site reflect very well the size difference between Ba and Sn, considering the covalent radius.

We assumed the overall occupation of Ba, Rb, and

TABLE I: Crystal data and structure refinement for Rb and Sn substituted BaFe₂As₂.

| | |
|---|--|
| Crystallographic formula (XRD) | Ba _{0.89} Rb _{0.05} Sn _{0.06} Fe ₂ As ₂ |
| Temperature (K) | 295(2) |
| Wavelength (Å) | 0.71073/Mo-K α |
| Crystal system, space group, Z | Tetragonal, $I4/mmm$, 2 |
| Unit cell dimensions (Å) | $a = 3.9250(2)$, $c = 13.2096(5)$ |
| Volume (Å ³) | 203.502(3) |
| Calculated density (g/cm ³) | 6.449 |
| Absorption correction type | analytical |
| Absorption coefficient (mm ⁻¹) | 32.413 |
| $F(000)$ | 345 |
| Crystal size (μm^3) | 117 x 77 x 18 |
| θ range for data collection | 5.42 to 42.81 deg |
| Index ranges | $-6 \leq h \leq 7$, $-7 \leq k \leq 6$, $-26 \leq l \leq 7$ |
| Reflections collected/unique | 1626/291 $R_{\text{int}} = 0.0458$ |
| Completeness to 2θ | 96.4 % |
| Refinement method | Full-matrix least-squares on F^2 |
| Data/restraints/parameters | 291/0/13 |
| Goodness-of-fit on F^2 | 1.052 |
| Final R indices [$I > 2\sigma(I)$] | $R_1 = 0.0389$, $wR_2 = 0.1106$ |
| R indices (all data) | $R_1 = 0.0414$, $wR_2 = 0.1122$ |
| $\Delta\rho_{\text{max}}$ and $\Delta\rho_{\text{min}}$ (e/Å ³) | 5.848 and -3.457 |
| Bond lengths (Å) | |
| Ba/Rb-As | 3.3774(3) x 8 |
| Fe-As | 2.3979(3) x 4 |
| Fe-Fe | 2.7754(1) x 4 |
| As-Sn | 2.894(3) x 4 |
| Fe-Sn | 2.945(7) x 4 |
| Bond angles (deg) | |
| As-Fe-As | 109.86(2) |
| | 109.28(1) |

TABLE II: Atomic coordinates, occupancy factors, and equivalent isotropic and anisotropic displacement parameters [$\text{\AA}^2 \times 10^3$] for Rb and Sn substituted BaFe_2As_2 .

| Atom | Site | x | y | z | $Occ.$ | U_{iso} | $U_{11} = U_{22}$ | U_{33} |
|--------|------|-----|-----|-----------|------------|-----------|-------------------|----------|
| Ba(Rb) | 2a | 0 | 0 | 0 | 0.89(0.05) | 17(1) | 17(1) | 17(1) |
| Sn | 4e | 0 | 0 | 0.0837(7) | 0.06 | 10(3) | 13(4) | 5(3) |
| As | 4e | 0 | 0 | 0.3543(1) | 1 | 12(1) | 11(1) | 15(1) |
| Fe | 4d | 0.5 | 0 | 0.25 | 1 | 12(1) | 9(1) | 17(1) |

U_{iso} is defined as one third of the trace of the orthogonalized U_{ij} tensor. The anisotropic displacement factor exponent takes the form: $-2\pi^2 \cdot (h^2 a^2 \cdot U_{11} + \dots + 2hka b \cdot U_{12})$. For symmetry reasons $U_{23} = U_{13} = U_{12} = 0$.

Sn to be 100 %. The Sn occupation was also refined and found to be ~ 6 % of the Ba/Rb/Sn sites. The Sn content of 1.2 ± 0.3 at.% agrees with the EDX data (1.7 at.%). The results of structure refinement are presented in the Tables 1 and 2. The resulting structure is shown in Fig. 4. Compared to unsubstituted BaFe_2As_2 the lattice parameter a is slightly shorter, the c parameter is longer and the volume of the unit cell is smaller too.²³ A similar tendency has been observed for other “122” compounds, when Ba or Sr is replaced by K.^{8,26,27} The increase of the c parameter in the studied crystals $\text{Ba}_{0.84}\text{Rb}_{0.10}\text{Sn}_{0.09}\text{Fe}_2\text{As}_{1.96}$ is caused mainly by substitution of Ba^{2+} ions ($r = 1.42$ \AA) by larger Rb^+ ions ($r = 1.61$ \AA).²⁸ The relatively marked shortening of the a parameter (larger than expected from Vegard’s law) seems to be caused by Sn incorporation.

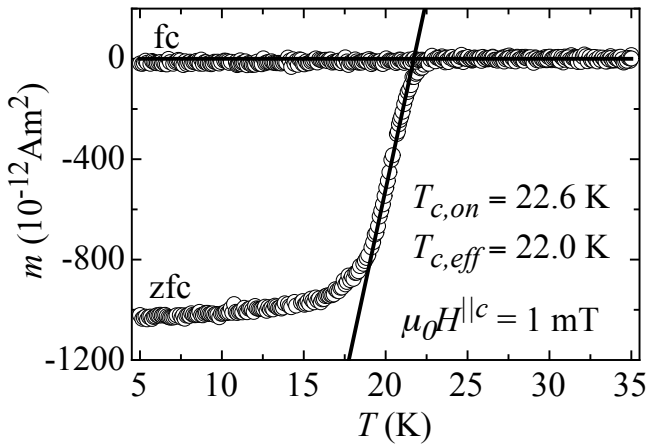


FIG. 5: Temperature dependence (field-cooled and zero-field-cooled) of the magnetic moment in a magnetic field of 1 mT applied parallel to the c -axis on the $\text{Ba}_{0.84}\text{Rb}_{0.10}\text{Sn}_{0.09}\text{Fe}_2\text{As}_{1.96}$ crystal with a volume of about $1.56 \cdot 10^{-13} \text{ m}^3$.

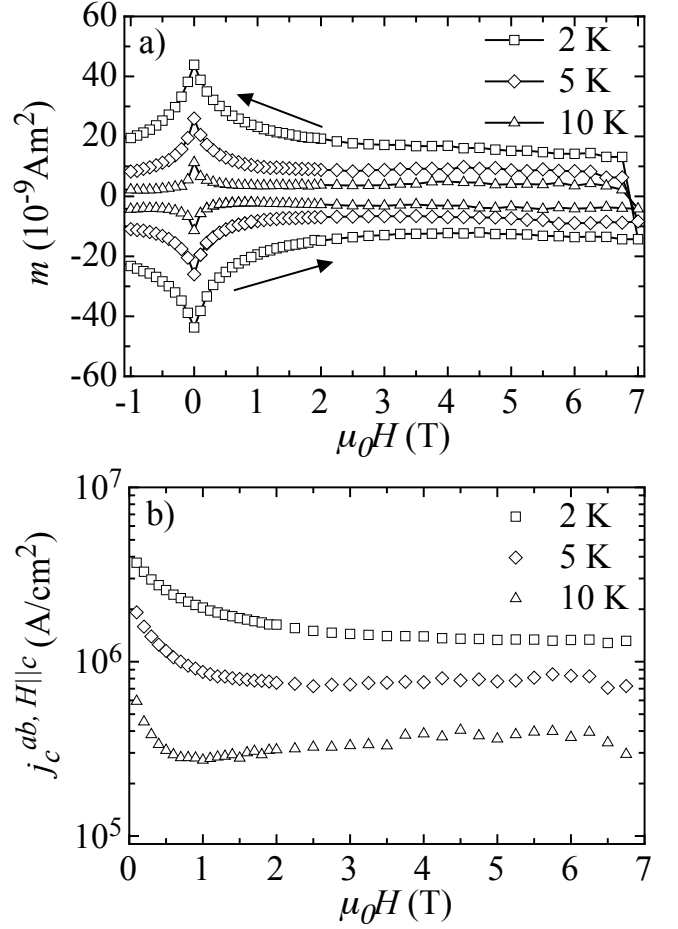


FIG. 6: a) Magnetic hysteresis loops measured at 2 K, 5 K, and 10 K in a field up to 7 T parallel to the c -axis on the $\text{Ba}_{0.84}\text{Rb}_{0.10}\text{Sn}_{0.09}\text{Fe}_2\text{As}_{1.96}$ crystal with a volume of about $1.56 \cdot 10^{-13} \text{ m}^3$ and with dimensions of $125 \times 125 \mu\text{m}^2$ in the plane perpendicular to the applied magnetic field. b) The critical current density calculated from the hysteresis loops.

B. Critical current density and irreversibility line

A plate like single crystal from the same batch and therefore identical lattice parameters with approximate dimensions of $125 \times 125 \times 10 \mu\text{m}^3$ was chosen for DC magnetization and for magnetic torque studies. In Fig. 5 we show the susceptibility measured in a magnetic field of 1 mT parallel to the crystallographic c -axis, showing a narrow transition with an effective transition temperature around 22 K and with an onset to superconductivity at 22.6 K.

The low temperature signal recorded in the zero-field-cooled mode corresponds to a full diamagnetic response. The observed extremely small magnetic moment in the field-cooled mode is due to the pronounced magnetic irreversibility, possibly due to the local lattice distortions caused by the substitution with relatively big Rb ions, introducing effective pinning centers.

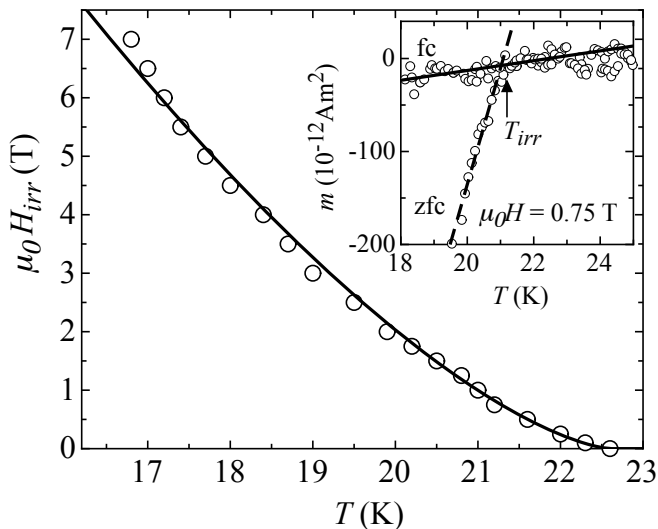


FIG. 7: Temperature dependence of the irreversibility field H_{irr} for $\text{Ba}_{0.84}\text{Rb}_{0.10}\text{Sn}_{0.09}\text{Fe}_2\text{As}_{1.96}$ for $H||c$. The inset illustrates how the quantity was determined. The irreversibility line is approximated very well by a power-law temperature dependence with an exponent $3/2$ (solid line), as discussed in the text.

A relatively strong pinning was confirmed in magnetic hysteresis loop measurements (see Figs. 6a, 6b, and 7) and by magnetic torque, as discussed later. The critical current density at 2 K, 5 K, and 10 K, estimated from the field dependence of the magnetic moment using Bean's model,^{29,30} reaches values of the order of 10^6 A/cm² (see Fig. 6b), which is very promising for applications. Similar values for the critical current were reported for BaFe_2As_2 substituted with K.³¹ The slight increase of the critical current density with increasing field in Fig. 6b is most likely due to the peak effect, which results in an effective increase of the irreversibility in the $M(H)$ curves (see Fig. 6a). Numerous explanations have been proposed, relying the effect to an increase in the microscopic pinning force, matching effects, field induced granularity or pinning site activation, crossover of pinning regimes, or a phase transition in vortex matter. All models include a field dependent flux-creep rate and a critical current density that decreases monotonically with increasing magnetic field.³²

From temperature dependent magnetization measurements at various magnetic fields we deduced the irreversibility line $H_{irr}(T)$ by following the temperatures for which the zero-field-cooled and field-cooled branches merge. The results are plotted in Fig. 7, where the upper inset to the figure illustrates the derivation in a magnetic field of 0.75 T. The irreversibility line is located in relatively high magnetic fields. A similar behavior has been reported for K substituted BaFe_2As_2 .³¹

The irreversibility line for $\text{Ba}_{0.84}\text{Rb}_{0.10}\text{Sn}_{0.09}\text{Fe}_2\text{As}_{1.96}$ is very well described by a power-law temperature

dependence according to $(1 - T/T_c)^n$ with fitted parameters $T_c = 22.6(2)\text{K}$ and $n = 1.47(5)$ (see the straight line in the log-log H_{irr} vs. $(1 - T/T_c)$ dependence in Fig. 8). The value of $n = 1.47(5)$ is very close to $n = 3/2$, typical for high- T_c superconductors characterized by an unusually small coherence length and an exceptionally high thermal activation at high temperatures.³³ A comparison of the irreversibility lines is presented in Fig. 8: single crystal of $\text{Ba}_{0.84}\text{Rb}_{0.10}\text{Sn}_{0.09}\text{Fe}_2\text{As}_{1.96}$, high- T_c $\text{YBa}_2\text{Cu}_3\text{O}_{7-\delta}$,³⁴ $\text{La}_{1.86}\text{Sr}_{0.14}\text{CuO}_4$,³⁵ $\text{Bi}_2\text{Sr}_2\text{CaCu}_2\text{O}_{8+\delta}$ single crystals,³⁶ and $\text{HgBa}_2\text{Ca}_2\text{Cu}_3\text{O}_{8+\delta}$ single crystal with strong pinning centers intentionally introduced by neutron irradiation.³⁷ The irreversibility line for $\text{Ba}_{0.84}\text{Rb}_{0.10}\text{Sn}_{0.09}\text{Fe}_2\text{As}_{1.96}$ is located in significantly higher magnetic fields and temperatures than those of $\text{La}_{1.86}\text{Sr}_{0.14}\text{CuO}_4$, $\text{Bi}_2\text{Sr}_2\text{CaCu}_2\text{O}_{8+\delta}$, and $\text{HgBa}_2\text{Ca}_2\text{Cu}_3\text{O}_{8+\delta}$. Its position in the reduced temperature phase diagram is comparable only with that one for $\text{YBa}_2\text{Cu}_3\text{O}_{7-\delta}$, i.e., with the position of the irreversibility line for the high- T_c superconductor characterized by the lowest anisotropy value among the compounds compared here ($\gamma \sim 6$). Furthermore, the power-law exponents describing the irreversibility lines for both $\text{Ba}_{0.84}\text{Rb}_{0.10}\text{Sn}_{0.09}\text{Fe}_2\text{As}_{1.96}$ and $\text{YBa}_2\text{Cu}_3\text{O}_{7-\delta}$ are essentially identical (see the parallel lines in Fig. 8).

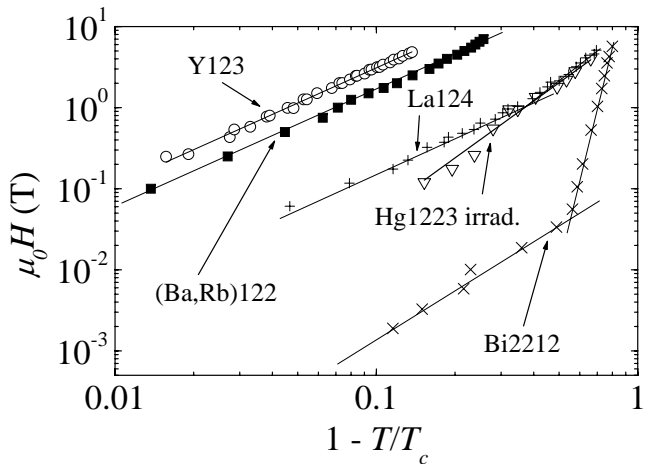


FIG. 8: Comparison of the irreversibility line for the $\text{Ba}_{0.84}\text{Rb}_{0.10}\text{Sn}_{0.09}\text{Fe}_2\text{As}_{1.96}$ single crystal for $H||c$ -axis [(Ba,Rb)122] with those for $\text{YBa}_2\text{Cu}_3\text{O}_{7-\delta}$ [Y123],³⁴ $\text{La}_{1.86}\text{Sr}_{0.14}\text{CuO}_4$ [La124],³⁵ $\text{Bi}_2\text{Sr}_2\text{CaCu}_2\text{O}_{8+\delta}$ single crystals [Bi2212]³⁶ and with $\text{HgBa}_2\text{Ca}_2\text{Cu}_3\text{O}_{8+\delta}$ single crystal with strong pinning centers intentionally introduced by neutron irradiation [Hg1223 irr.].³⁷ The solid lines are fits to a power-law dependence as explained in the text.

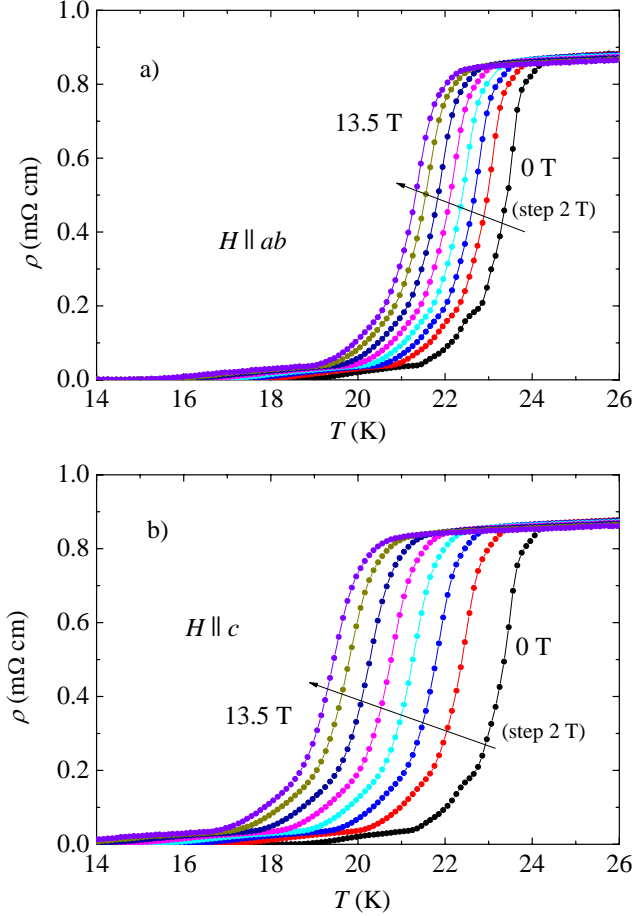


FIG. 9: (Color online) Examples of $\rho(T, H)$ dependences measured on the $\text{Ba}_{0.84}\text{Rb}_{0.10}\text{Sn}_{0.09}\text{Fe}_2\text{As}_{1.96}$ crystal with the field applied parallel to the (Fe_2As_2) -layers ($H||ab$) (a) and perpendicular to them ($H||c$) (b) in magnetic fields of 0, 2, 4, 6, 8, 10, 12, and 13.5 T. The solid lines are guides to the eye.

C. Upper critical field and superconducting state anisotropy

The electronic anisotropy is a determining factor for the behavior of a superconductor in an applied magnetic field, and thus is also of importance when possible applications are considered. We have estimated the anisotropy from the shift of the resistive transition as well as from magnetic torque measurements, leading to consistent results.

The resistance has been measured with the magnetic field applied parallel to the (Fe_2As_2) -layers ($H||ab, I||H$) and perpendicular to them ($H||c, I||ab$). Examples of $\rho(T, H)$ are shown in Fig. 9. Particularly notable is the well defined shift of the resistance drop with increasing field, without a significant broadening due to flux flow dissipation. In several of the larger crystals used for resistance measurements, the resistance drop proceeds in two or three steps, indicative of the presence of two or

more distinct parts of the crystal with distinct transition temperatures. Yet, each of the steps can be followed as a function of field yielding very similar and consistent slopes of the upper critical field.

As the resistive transitions are not markedly broadened, we define $T_c(H)$ as the temperature where the resistance has decreased to 50 % (see Fig. 10). For $H||ab$ the upper critical field $H_{c2}^{||ab}$ increases with a slope of 7.1(3) T/K with a clearly visible rounding near T_c , whereas $H_{c2}^{||c}$ increases with a slope of 4.2(2) T/K again exhibiting an upturn near T_c where thermal phase fluctuations are expected to influence its determination. The upper critical slope $\mu_0 dH_{c2}^{||c}/dT$ is considerably higher than in $\text{YBa}_2\text{Cu}_3\text{O}_{7-\delta}$ (1.9 T/K),³⁸ in $\text{HgBa}_2\text{Ca}_2\text{Cu}_3\text{O}_{8+\delta}$ (2 T/K),³⁹ in unsubstituted MgB_2 (0.12 T/K),⁴⁰ and in $\text{LaFeAsO}_{0.89}\text{F}_{0.11}$ (2 T/K).⁴¹ This steep slope also points to a very high $H_{c2}^{||c}(T = 0)$. The upper critical field anisotropy in the vicinity of T_c , defined as $\gamma_H = H_{c2}^{||ab}/H_{c2}^{||c}$, (inset to the Fig. 10) decreases with decreasing temperature, a similar trend as observed in the “1111” pnictides.⁴² This suggests similar temperature dependences of the anisotropic parameters among different classes of pnictides.⁴³ However, it should be noted that the values for the upper critical field anisotropy are significantly smaller in the “122” class ($\sim 2.5 - 3$) than in the “1111” group of superconductors ($\sim 5 - 6$), with a T_c of ~ 45 K.⁴²

A very important difference between the behavior of the “122” and “1111” iron-pnictide superconductors should be pointed out. While $(\text{Ba,Rb})122$ shows a sharp transition and a clear onset of superconductivity, there is no sharp transition for “1111” superconductors.⁴² Therefore, $T_c(H)$ for “1111” superconductors is less clearly defined and the determination of $H_{c2}(T)$ and its anisotropy

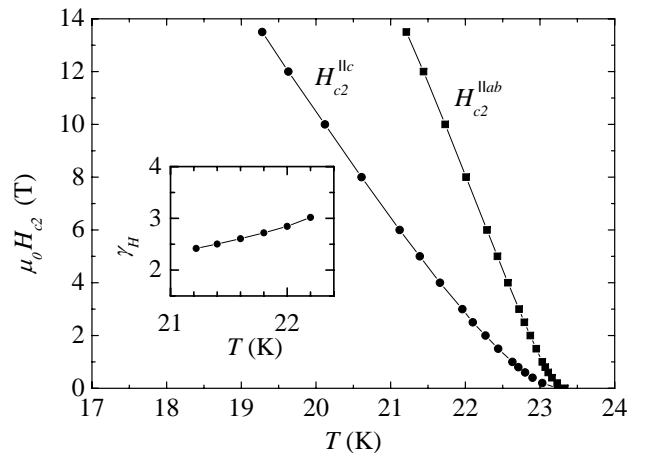


FIG. 10: Temperature dependence of the upper critical field with $H||ab$ and with $H||c$ for $\text{Ba}_{0.84}\text{Rb}_{0.10}\text{Sn}_{0.09}\text{Fe}_2\text{As}_{1.96}$. The solid lines are guides to the eye. Inset: The upper critical field anisotropy $\gamma_H = H_{c2}^{||ab}/H_{c2}^{||c}$ in the vicinity of T_c .

$\gamma_H(T)$ in the vicinity of T_c is criterion dependent. The results of high field resistivity measurements by Jaroszynski *et al.*⁴² indicate that the upper critical field anisotropy becomes criterion independent for temperatures of about 10 K below T_c only, providing convincing evidence for the temperature dependent anisotropy in “1111” superconductors for the limited temperature range of $\sim 10 - 17$ K below T_c . In contrast, the resistance drop at T_c in the (Ba,Rb)122 crystals remains essentially unaffected by high magnetic fields and, therefore, provides for a reliable determination of $H_{c2}(T)$. Accordingly, the upper critical field anisotropy $\gamma_H(T)$ is well defined too (see Figs. 9 and 10).

Estimating $H_{c2}(0)$ from extrapolations of the present data, covering a limited temperature range, is inappropriate not only due to the curvature of $H_{c2}(T)$, but more importantly because of the two-band nature of superconductivity. Nevertheless, if one would disregard these considerations, the simple Werthamer-Helfand-Hohenberg (WHH) extrapolation⁴⁴ would give values of $\mu_0 H_{c2}^{\parallel c}(0) \simeq 70(5)$ T and $\mu_0 H_{c2}^{\parallel ab}(0) \simeq 120(6)$ T.

Torque measurements were performed in the temperature range close to T_c , where the pronounced irreversibility leads to only minor distortions of the torque. For minimizing pinning effects, the mean (reversible) torque, $\tau_{rev} = (\tau(\theta^+) + \tau(\theta^-))/2$ was calculated from measurements with counterclockwise and clockwise rotating of the magnetic field around the sample, as indicated by the black open diamonds in Fig. 11. Unfortunately, due to the small superconducting torque signal a big background component is contributing a pronounced additional signal to the torque. This sinusoidal component has been included by an additional sinusoidal function in the fitting model after Kogan *et al.*^{45,46}

$$\tau(\theta) = -\frac{V\Phi_0 H}{16\pi\lambda_{ab}^2} \left(1 - \frac{1}{\gamma^2}\right) \frac{\sin(2\theta)}{\epsilon(\theta)} \ln \left(\frac{\eta H_{c2}^{\parallel c}}{\epsilon(\theta)H} \right) + A \sin(2\theta), \quad (1)$$

where V is the volume of the crystal, Φ_0 is the elementary flux quantum, γ denotes the superconducting state anisotropy parameter, λ_{ab} the in-plane component of the magnetic penetration depth, $H_{c2}^{\parallel c}$ the upper critical field along the c -axis of the crystal, η denotes a numerical parameter of the order of unity depending on the structure of the flux-line lattice, A is the amplitude of the background torque, and $\epsilon(\theta) = [\cos^2(\theta) + \gamma^{-2} \sin^2(\theta)]^{1/2}$.

The superconducting state anisotropy parameter γ , fitted to the mean torque data is found to be $2.8(4)$ near T_c in very good agreement with the estimate of γ_H from resistivity measurements shown in Fig. 10. Due to the low anisotropy, the strong irreversibility and the pronounced normal state background, no temperature dependent study of the anisotropy parameter was performed. It is highly gratifying to find excellent agreement among the two ways for estimating the electronic anisotropy in the vicinity of T_c , where independently of the predictions for the detailed electronic structure, all of the

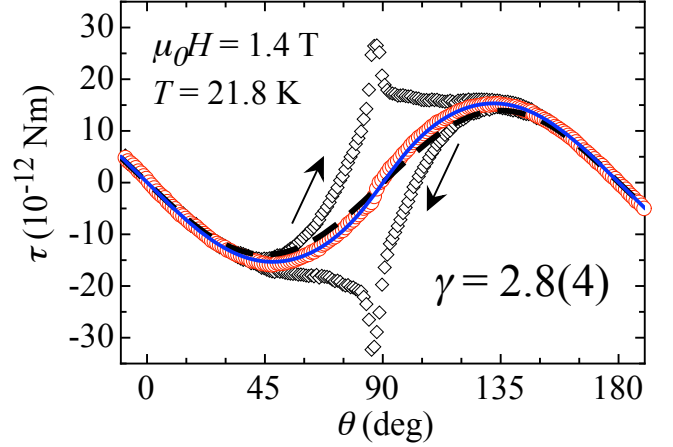


FIG. 11: (Color online) Angular dependence of the raw (black open diamonds) and the reversible (open circles) torque of the $\text{Ba}_{0.84}\text{Rb}_{0.10}\text{Sn}_{0.09}\text{Fe}_2\text{As}_{1.96}$ single crystal in the superconducting state at $T = 21.8$ K and in $\mu_0 H = 1.4$ T. The solid line is given by the Kogan model (Eq. (1)) with the parameters fitted to the reversible torque data (open circles). A very big background component contributes a pronounced signal to the torque and is shown by dashed line.

electronic anisotropies should coincide. Obviously, superconducting $\text{Ba}_{0.84}\text{Rb}_{0.10}\text{Sn}_{0.09}\text{Fe}_2\text{As}_{1.96}$ is much more isotropic than $\text{SmFeAsO}_{0.8}\text{F}_{0.2}$ and $\text{NdFeAsO}_{0.8}\text{F}_{0.2}$, where reliable anisotropy parameter values up to 20 can be derived.^{25,43} The anisotropy parameter measured for $\text{Ba}_{0.84}\text{Rb}_{0.10}\text{Sn}_{0.09}\text{Fe}_2\text{As}_{1.96}$ is much smaller than those typical for high- T_c superconductors, but it is quite similar to those reported for $\text{Ba}_{1-x}\text{K}_x\text{Fe}_2\text{As}_2$ and $\text{Sr}_{1-x}\text{K}_x\text{Fe}_2\text{As}_2$ ^{20,47,48}. The electronic coupling of the Fe_2As_2 layers through the intervening (Ba, Rb) layers is more effective than through the LnO layers in the “1111” class of superconductors.

D. Effect of Sn incorporation

The effect of Sn incorporation on the properties of AFe_2As_2 has not been studied in detail. Single crystals of BaFe_2As_2 grown from Sn flux reveal the structural and magnetic phase transition at significantly lower temperature (85 K)²⁰ than Sn-free material (140 K) although the magnetic structure is virtually the same.⁴⁹ The electrical resistivity (below the tetragonal-orthorhombic transition) for BaFe_2As_2 with 1% Sn increases upon decreasing temperature²⁰ while for pure BaFe_2As_2 crystals $\rho(T)$ is typical for metals.⁵⁰ It is worth noting that although Sn incorporation lowers the structural transition temperature in BaFe_2As_2 it does not lead to superconductivity. The effect of Sn incorporation in superconducting alkali metal-substituted BaFe_2As_2 seems to be fully masked by the much stronger effect of the alkali metal doping.

IV. SUMMARY

Single crystals of $\text{Ba}_{1-x}\text{Rb}_x\text{Fe}_2\text{As}_2$ ($x = 0.05\text{--}0.1$) have been grown and their crystallographic and basic superconducting state properties were presented. This is the first example of superconductivity induced by Rb substitution in this family of materials. It was found that the irreversibility line is located in relatively high magnetic fields comparable to the one for $\text{YBa}_2\text{Cu}_3\text{O}_{7-\delta}$ only, i.e. for the high- T_c superconductor with the lowest anisotropy. The electronic anisotropy, derived consistently from resistance and from magnetic torque measurements, ranges from ~ 3 near T_c to lower values at lower temperatures, and indicates that $\text{Ba}_{1-x}\text{Rb}_x\text{Fe}_2\text{As}_2$ is electronically much more isotropic

than $\text{SmFeAsO}_{0.8}\text{F}_{0.2}$ and $\text{NdFeAsO}_{0.8}\text{F}_{0.2}$. The critical current density at 5 K exceeds 10^6 A/cm², which together with the high upper critical fields, is very promising for applications.

V. ACKNOWLEDGMENTS

We would like to thank P. Wägli for the EDX analysis. This work was supported by the Swiss National Science Foundation, by the NCCR program MaNEP, and partially by the Polish Ministry of Science and Higher Education within the research project for the years 2007-2009 (No. N N202 4132 33).

-
- * Electronic address: bukowski@phys.ethz.ch
- ¹ Y. Kamihara, H. Hiramatsu, M. Hirano, R. Kawamura, H. Yangi, T. Kamiya, and H. Hosono, *J. Am. Chem. Soc.* **128**, 10012 (2006).
 - ² Y. Kamihara, T. Watanabe, M. Hirano, and H. Hosono, *J. Am. Chem. Soc.* **130**, 3296 (2008).
 - ³ Z.-A. Ren, W. Lu, J. Yang, W. Yi, X.-L. Shen, Z.-C. Li, G.-C. Che, X.-L. Dong, L.-L. Sun, F. Zhou, Z.-X. Zhao, *Chin. Phys. Lett.* **25**, 2215 (2008).
 - ⁴ H. Okada, K. Igawa, H. Takahashi, Y. Kamihara, M. Hirano, H. Hosono, K. Matsubayashi, and Y. Uwatoko, *J. Phys. Soc. Jap.* **77**, 113712 (2008).
 - ⁵ C. Wang, L. Li, S. Chi, Z. Zhu, Z. Ren, Y. Li, Y. Wang, X. Lin, Y. Luo, S. Jiang, X. Xu, G. Cao, and Z. Xu, *Europhys. Lett.* **83**, 67006 (2008).
 - ⁶ H.-H. Wen, G. Mu, L. Fang, H. Yang, and X. Zhu, *Europhys. Lett.*, **82**, 17009 (2008).
 - ⁷ M. Rotter, M. Tegel, and D. Johrendt, *Phys. Rev. Lett.* **101**, 107006 (2008).
 - ⁸ K. Sasmal, B. Lv, B. Lorenz, A. M. Guloy, F. Chen, Y.-Y. Xue, and C.-W. Chu, *Phys. Rev. Lett.* **101**, 107007 (2008).
 - ⁹ G. Wu, H. Chen, T. Wu, Y. L. Xie, Y. J. Yan, R. H. Liu, X. F. Wang, J. J. Ying, and X. H. Chen, *J. Phys.: Condens. Matter* **20**, 422201 (2008).
 - ¹⁰ H. S. Jeevan, Z. Hossain, D. Kasinathan, H. Rosner, C. Geibel, and P. Gegenwart, *Phys. Rev. B* **78**, 092406 (2008).
 - ¹¹ Y. Qi, Z. Gao, L. Wang, D. Wang, X. Zhang, and Y. Ma, *New Journal of Physics* **10**, 123003 (2008).
 - ¹² A. S. Sefat, R. Jin, M. A. McGuire, B. C. Sales, D. J. Singh, and D. Mandrus, *Phys. Rev. Lett.* **101**, 117004 (2008).
 - ¹³ A. Leithe-Jasper, W. Schnelle, C. Geibel, and H. Rosner, *Phys. Rev. Lett.* **101**, 207004 (2008).
 - ¹⁴ L. J. Li, Q. B. Wang, Y. K. Luo, H. Chen, Q. Tao, Y. K. Li, X. Lin, M. He, Z. W. Zhu, G. H. Cao, and Z. A. Xu, *New. J. Phys.* **11**, 025008 (2009).
 - ¹⁵ T. Park, E. Park, H. Lee, T. Klimczuk, E. D. Bauer, F. Ronning, and J. D. Thompson, *J. Phys.: Condens. Matter* **20**, 322204 (2008).
 - ¹⁶ M. S. Torikachvili, S. L. Budko, N. Ni, and P. C. Canfield, *Phys. Rev. Lett.* **101**, 057006 (2008).
 - ¹⁷ K. Igawa, H. Okada, H. Takahashi, S. Matsuishi, Y. Kamihara, M. Hirano, H. Hosono, K. Matsubayashi, and Y. Uwatoko, *J. Phys. Soc. Jpn.* **78**, 025001 (2009).
 - ¹⁸ P. L. Alireza, Y. T. C. Ko, J. Gillett, C. M. Petrone, J. M. Cole, S. E. Sebastian, and G. G. Lonzarich, *J. Phys.: Condens. Matter* **21** 012208 (2009).
 - ¹⁹ P. Wenz and H. U. Schuster, *Z. Naturforsch., B: Anorg. Chem., Org. Chem.* **39**, 1816 (1984).
 - ²⁰ N. Ni, S. L. Budko, A. Kreyssig, S. Nandi, G. E. Rustan, A. I. Goldman, S. Gupta, J. D. Corbett, A. Kracher, and P. C. Canfield, *Phys. Rev. B* **78**, 014507 (2008).
 - ²¹ Oxford Diffraction Ltd. XCalibur, CrysAlis Software System, Version 1.171.32.15 (release 10-01-2008).
 - ²² G. Sheldrick, *SHELXL-97: Program for the Refinement of Crystal Structures*, University of Göttingen, Germany, 1997.
 - ²³ M. Rotter, M. Tegel, D. Johrendt, I. Schellenberg, W. Hermes, and R. Pöttgen, *Phys. Rev. B* **78**, 020503(R) (2008).
 - ²⁴ S. Kohout, J. Roos, and H. Keller, *Rev. Sci. Instr.* **78**, 013903 (2007).
 - ²⁵ S. Weyeneth, R. Puzniak, U. Mosele, N. D. Zhigadlo, S. Katrych, Z. Bukowski, J. Karpinski, S. Kohout, J. Roos, and H. Keller, *J. Supercond. Nov. Magn.* **22**, 325 (2009).
 - ²⁶ H. Chen, Y. Ren, Y. Qiu, W. Bao, R. H. Liu, G. Wu, T. Wu, Y. L. Xie, X. F. Wang, Q. Huang, and X. H. Chen, *Europhys. Lett.* **85**, 17006 (2009).
 - ²⁷ M. Rotter, M. Pangerl, M. Tegel, and D. Johrendt, *Angeordnete Chemie-International Edition* **47**, 7949 (2008).
 - ²⁸ R. D. Shannon, *Acta Crystallographica* **A32**, 751 (1976).
 - ²⁹ C. P. Bean, *Phys. Rev. Lett.* **8**, 250 (1962).
 - ³⁰ C. P. Bean, *Rev. Mod. Phys.* **36**, 31 (1964).
 - ³¹ H. Yang, H. Luo, Z. Wang, and H.-H. Wen, *Appl. Phys. Lett.* **93**, 142506 (2008).
 - ³² M. Werner, F. M. Sauerzopf, H. W. Weber, and A. Wisniewski, *Phys. Rev. B* **61**, 14795 (2000).
 - ³³ Y. Yeshurun and A. P. Malozemoff, *Phys. Rev. Lett.* **60**, 2202 (1988).
 - ³⁴ A. Schilling, H. R. Ott, and Th. Wolf, *Phys. Rev. B* **46**, 14253 (1992).
 - ³⁵ A. Schilling, R. Jin, J. D. Guo, H. R. Ott, I. Tanaka, and H. Kojima, *Physica B* **194-196**, 1555 (1994).
 - ³⁶ J. Ricketts, R. Puzniak, C.-J. Liu, G. D. Gu, N. Koshizuka, and H. Yamauchi, *Appl. Phys. Lett.* **65**, 3284 (1994).
 - ³⁷ A. Wisniewski, R. Puzniak, J. Karpinski, J. Hofer, R. Szymczak, M. Baran, F. M. Sauerzopf, R. Molinski, E. M. Kopnin, and J. R. Thompson, *Phys. Rev. B* **61**, 791

- (2000).
- ³⁸ U. Welp, W. K. Kwok, G. W. Crabtree, K. G. Vandervoort, and J. Z. Liu, Phys. Rev. Lett. **62**, 1908 (1989).
 - ³⁹ A. Schilling, O. Jeandupeux, S. Büchi, H. R. Ott, and C. Rossel, Physica C **235-240**, 229 (1994).
 - ⁴⁰ M. Angst, R. Puzniak, A. Wisniewski, J. Jun, S. M. Kazakov, J. Karpinski, J. Roos, and H. Keller, Phys. Rev. Lett. **88**, 167004 (2002).
 - ⁴¹ F. Hunte, J. Jaroszynski, A. Gurevich, D. C. Larbalestier, R. Jin, A. S. Sefat, M. A. McGuire, B. C. Sales, D. K. Christen, and D. Mandrus, Nature **453**, 903 (2008).
 - ⁴² J. Jaroszynski, F. Hunte, L. Balicas, Y.-J. Jo, I. Raicevic, A. Gurevich, D. C. Larbalestier, F. F. Balakirev, L. Fang, P. Cheng, Y. Jia, and H.-H. Wen, Phys. Rev. B **78**, 174523 (2008).
 - ⁴³ S. Weyeneth, R. Puzniak, N. D. Zhigadlo, S. Katrych, Z. Bukowski, J. Karpinski, and H. Keller, J. Supercond. Nov. Magn. **22**, 347 (2009).
 - ⁴⁴ N. R. Werthamer, E. Helfand, and P. C. Hohenberg, Phys. Rev. **147**, 295 (1966).
 - ⁴⁵ V. G. Kogan, Phys. Rev. B **24**, 1572 (1981).
 - ⁴⁶ V. G. Kogan, M. M. Fang, and S. Mitra, Phys. Rev. B **38**, 11958 (1988).
 - ⁴⁷ H. Q. Yuan, J. Singleton, F. F. Balakirev, S. A. Baily, G. F. Chen, J. L. Luo, and N. L. Wang, Nature **457**, 565 (2009).
 - ⁴⁸ G. F. Chen, Z. Li, J. Dong, G. Li, W. Z. Hu, X. D. Zhang, X. H. Song, P. Zheng, N. L. Wang, and J. L. Luo, Phys. Rev. B **78**, 224512 (2008).
 - ⁴⁹ Y. Su, P. Link, A. Schneidewind, Th. Wolf, P. Adelman, Y. Xiao, M. Meven, R. Mittal, M. Rotter, D. Johrendt, Th. Brueckel, and M. Loewenhaupt, Phys. Rev. B **79**, 064504 (2009).
 - ⁵⁰ X. F. Wang, T. Wu, G. Wu, H. Chen, Y. L. Xie, J. J. Ying, Y. J. Yan, R. H. Liu, and X. H. Chen arXiv:0806.2452v1, to be published in Phys. Rev. Lett.